Supernovae and Other Transients in the OGLE-IV Magellanic Bridge Data[*]

S. K o z ł o w s k i[1], A. U d a l s k i[1], Ł. W y r z y k o w s k i[1,2], R. P o l e s k i[1,3],
P. P i e t r u k o w i c z[1], J. S k o w r o n[1], M. K. S z y m a ń s k i[1], M. K u b i a k[1],
G. P i e t r z y ń s k i[1,4], I. S o s z y ń s k i[1] and K. U l a c z y k[1]

[1] Warsaw University Observatory, Al. Ujazdowskie 4, 00-478 Warszawa, Poland
e-mail:(simkoz,udalski,lw,rpoleski,pietruk,jskowron,msz,mk,pietrzyn,soszynsk,kulaczyk)
@astrouw.edu.pl
[2] Institute of Astronomy, University of Cambridge, Madingley Road, Cambridge CB3
0HA, UK
[3] The Ohio State University, 140 W. 18th Avenue, Columbus, OH 43210, USA
[4] Departamento de Astronomia, Universidad de Concepción, Casilla 160-C, Concepción,
Chile

ABSTRACT

We analyze two years (mid-2010 to mid-2012) of OGLE-IV data covering ≈ 65 deg^2 of the Magellanic Bridge (the area between the Magellanic Clouds) and find 130 transient events including 126 supernovae (SNe), two foreground dwarf novae and another two SNe-like transients that turned out to be active galactic nuclei (AGNs). We show our SNe detection efficiency as a function of SN peak magnitude based on available SNe rate estimates. It is 100% for SNe peak magnitudes $I < 18.8$ mag and drops to 50% at $I \approx 19.7$ mag. With our current observing area between and around the Magellanic Clouds (≈ 600 deg^2), we expect to find 24 SNe peaking above $I < 18$ mag, 100 above $I < 19$ mag, and 340 above $I < 20$ mag, annually. We briefly introduce our on-line near-real-time detection system for SNe and other transients, the OGLE Transient Detection System.

Key words: *supernovae: general – Magellanic Clouds – Surveys*

1. Introduction

Supernovae (SNe) are gigantic stellar explosions marking the ultimate death of massive stars. They are extremely luminous, often outshining all stars of the host galaxy for a short period of time, making them excellent probes of the distant Universe, to $z \approx 1.7$ for SNe Type Ia (Riess *et al.* 2001), $z \approx 2.4$ for SNe Type II (Cooke *et al.* 2009), and $z \approx 3.9$ for super-luminous SNe (Cooke *et al.* 2012). Type Ia SNe, exploding white dwarfs, can be used as "standardizable" candles (*e.g.*, Phillips 1993). This yardstick redefined our view of the Universe, playing a

---

major role in discovering the accelerating expansion of the Universe (*e.g.*, Riess *et al.* 1998, Perlmutter *et al.* 1999). Recent studies use total samples of ≈ 600 SNe Type Ia to constrain evolution of the Universe (*e.g.*, Conley *et al.* 2011, Suzuki *et al.* 2012). Our understanding of the progenitors of SNe Type Ia, their hosts, and the connection between them remains limited as illustrated by the continuing debate over the relative roles of the single-degenerate (SD) and double-degenerate (DD) channels for producing them.

While core collapse SNe (ccSNe – Type II and Ibc) may also be "standardizable" candles (*e.g.*, Hamuy and Pinto 2002, Poznanski, Nugent and Filippenko 2010), they are primarily studied as probes of the evolution and death of massive stars (*e.g.*, Woosley and Weaver 1986, Smartt 2009) and for their role in providing the "feedback" that regulates star formation (*e.g.*, Silk 2005). Some important open questions are the death of higher mass progenitors of ccSNe (Kochanek *et al.* 2008, Smartt *et al.* 2009, Jennings *et al.* 2012), correlations of properties with metallicity (Prieto, Stanek, and Beacom 2008, Kozłowski *et al.* 2010b, Stoll *et al.* 2011), apparent correlations of pre-SN outbursts with the SN (*e.g.*, Pastorello *et al.* 2007) and the nature of the so-called SN impostors (Smith *et al.* 2011, Kochanek, Szczygieł and Stanek 2012). Many of these issues can be addressed by unbiased surveys for ccSNe.

In the early days of the Optical Gravitational Lensing Experiment (OGLE), we also searched for SNe in parallel with our successful microlensing searches (Udalski *et al.* 1993). Due to the small area of the CCD camera and the limited number of observing nights awarded on the 1.0 m Swope telescope this was not a competitive survey. We returned to the problem while implementing "The New Objects in the OGLE-III Sky" real-time system (NOOS; Udalski 2003) as part of the larger area OGLE-III survey, using the 1.3 m Warsaw telescope, discovering several dozen SNe over the years 2003–2005 (*e.g.*, Udalski 2004a,b).

In its fourth phase, the OGLE survey (OGLE-IV), also conducted on the 1.3 m Warsaw telescope, uses a 32 CCD mosaic camera covering 1.4 $\deg^2$. One of the OGLE-IV survey goals is to find variable stars in a wide area (≈ 600 $\deg^2$) around and between the Magellanic Clouds in order to study the spatial distribution of stars including Cepheids and RR Lyr stars (Soszyński *et al.* 2013, in preparation). On average, these areas have low stellar density and many galaxies are readily detected in our images (see Soszyński *et al.* 2012). With an observing cadence of 2–3 days, we find not only "regular" variable stars but also all types of transient events and active galactic nuclei (AGNs). While the OGLE-IV survey of the Magellanic Clouds was not specifically designed to find SNe, we are finding large numbers of them as a by-product (*e.g.*, Wyrzykowski, Udalski and Kozłowski 2012). Our goal is not to directly compete with dedicated SNe surveys, such as the Catalina Real-Time Transient Survey (CRTS; Drake *et al.* 2009), the Palomar Transient Factory (Law *et al.* 2009), the Supernova Legacy Survey (Astier *et al.* 2006), the Lick Observatory Supernova Search (LOSS, Li *et al.* 2011a,b), the Hubble Space Telescope Cluster

Supernova Survey (Suzuki *et al.* 2012), the CANDELS survey (Grogin *et al.* 2011, Koekemoer *et al.* 2011), but simply to contribute to the SN field with discoveries.

In this paper, we are interested in finding SNe amongst the variable OGLE-IV objects in the vicinity of the Magellanic Clouds. In Section 2, we describe the collected data, their analysis, and the methods to find SNe. The expected SNe numbers from known SNe rates as well as our detection efficiency is presented in Section 3. In Section 4, we describe the method of discriminating SNe from AGNs. A brief introduction to our near-real-time transient detection system can be found in Section 5. The paper is summarized and the data availability is described in Section 6.

2. Observational Data

The OGLE-IV survey is conducted with the 1.3 m Warsaw telescope located at the Las Campanas Observatory in Chile, operated by the Carnegie Institution for Science. In the current, fourth phase of the OGLE survey, the telescope is equipped with a mosaic camera composed of 32 CCD detectors, each having 2048×4102 pixels, totaling 268 mega-pixels. The new camera covers approximately 1.4 deg^2 of the sky with a scale of 0.26 arcsec/pixel. In this paper, we analyze the first
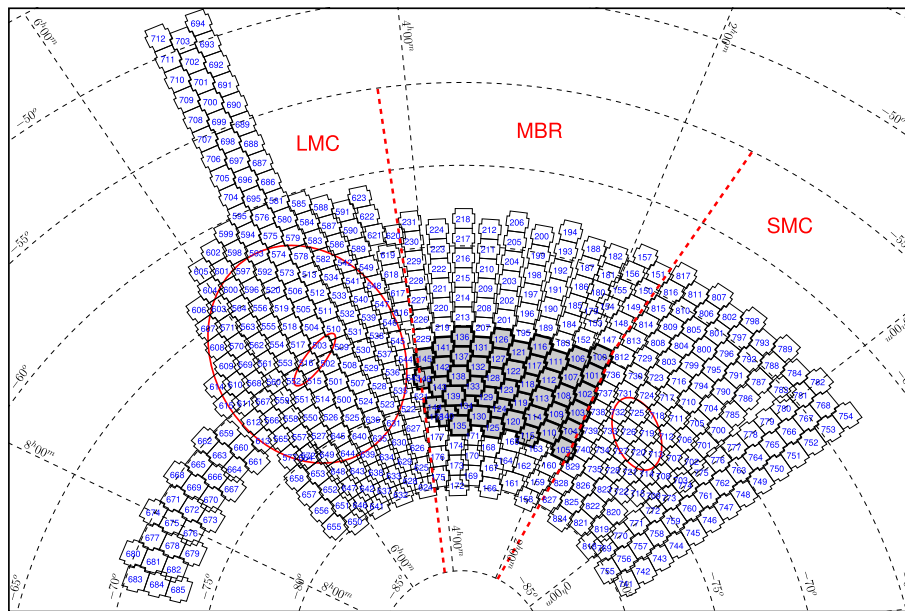
Fig. 1. Area of the Magellanic Clouds that has been monitored by OGLE-IV since 2012 is shown. Each labeled square-like shape corresponds to one 1.4 deg^2 OGLE-IV field. The early (2010–2012) monitored area of the Magellanic Bridge, analysis of which we report in this paper, is marked with thick lines (≈ 65 deg^2). The total current observed area is ≈ 600 deg^2. We schematically show the SMC (ellipse on the right) and the LMC's size and its bar (large and small ellipses on the left, respectively). Two nearly vertical dashed lines divide the LMC (*left*), MBR (*middle*), and SMC (*right*) areas.

two years (mid-2010 to mid-2012) of the Magellanic Bridge OGLE-IV data. This region consists of 47 slightly overlapping fields, covering a total of $\approx 65 \deg^2$ (Fig. 1). The median number of I-band points per $\approx$8-month-long season is 91, with an average cadence of 2.7 days. The seasonal gaps last ≈ 4 months.

The CCD frames are reduced on-the-fly at the telescope with the best-available bias and flat-field images. They are then fed to our own automatic difference image analysis (DIA technique; Woźniak 2000) photometric pipeline (Udalski *et al.* 2008). Each image of a given field is aligned to the corresponding template (reference) image, an average of high quality images, and the template is convolved and scaled to match the point spread function (PSF) flux and background, and then subtracted. The only remaining objects on the resulting difference image are real transient and variable objects, asteroids, satellite trails, cosmic rays, and noise.
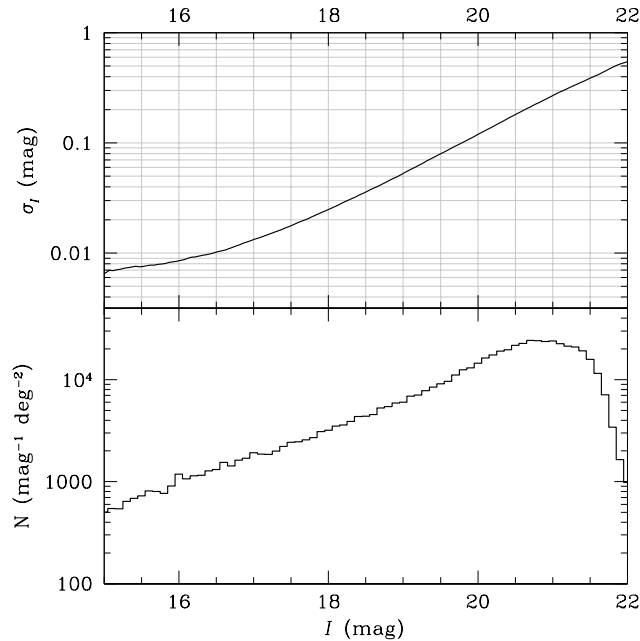
Fig. 2. Data statistics for central OGLE-IV MBR fields (MBR118 and MBR123). *Top:* Smoothed (three 0.05 mag bins) median dispersion for non-variable light curves as a function of I-band magnitude. *Bottom:* Histogram of the number of detected objects per magnitude per $\deg^2$. The detection of objects on the template image is complete to $I \approx 20.7$ mag. It then flattens out to $I \approx 21.3$ mag, and drops quickly to zero at about $I \approx 22.0$ mag. Transients from the database of new objects (appearing from below background) therefore come from progenitors/galaxies fainter than this limit.

The OGLE pipeline builds two databases. The first one is directly dependent on the template image. We detect all objects on the template image and then create light curves for each source by adding the flux measured for it on the difference image to the template flux. This is our standard database. The second database consists of new objects that are detected only on the difference images and have no counterparts on the template image within $0.''5$. In Fig. 2, we present the OGLE-

IV data quality – the median magnitude dispersion for non-variable objects as a function of magnitude and the number of detected objects on template images as a function of magnitude in low stellar density Magellanic Bridge fields.
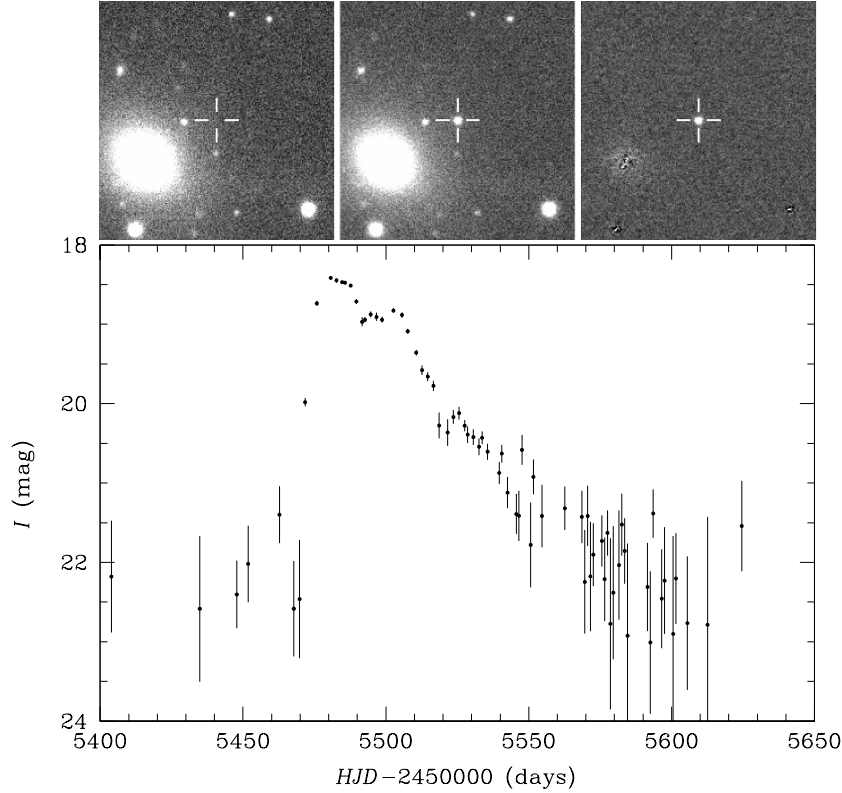
Fig. 3. *Top:* Finding chart for supernova OGLE-2010-SN-037 (MBR108.29.613). Each image covers $60'' \times 60''$. The *left image* shows the galaxy before the SN explosion, the *middle image* shows the SN at its peak (marked with cross hair), and the *right image* shows the difference image. The SN is located $21''5$ away from the elliptical galaxy 2MASX J02064540–7246329 at $z = 0.057$. *Bottom:* OGLE-IV light curve for OGLE-2010-SN-037. It peaked at $I = 18.41$ mag on 2010, October 11. The estimated absolute magnitude peak was $M_I \approx -18.7$ mag. Both the shape of the light curve and the peak absolute magnitude point to the SN Type Ia.

To search for SNe in the standard database, we adopted several parts of the method used in Wyrzykowski *et al.* (2009). For each epoch with magnitude $I_i \pm \Delta I_i$, we compute the significance of its variability by

$$\sigma_i = \frac{I_{\mathrm{med,B}} - I_i}{\sqrt{\Delta I_i^2 + \sigma_{\mathrm{B}}^2}} \tag{1}$$

with respect to the variability in an outer window B, spanning half of the data, and window A centered on the analyzed epoch. Here $I_{\mathrm{med,B}}$ and σ_{B} are the median and dispersion calculated in window B. We then searched for "bumps" defined as four

(three) consecutive data points with significance higher than 1.5 (1.8). The 63 201 light curves showing such bumps were then inspected visually. In the database of new objects, there were 8677 objects with at least three detections. We produced full light curves at the locations of these objects and then inspected them visually. We also carefully checked the template, original and subtracted images around peak and at the baseline.
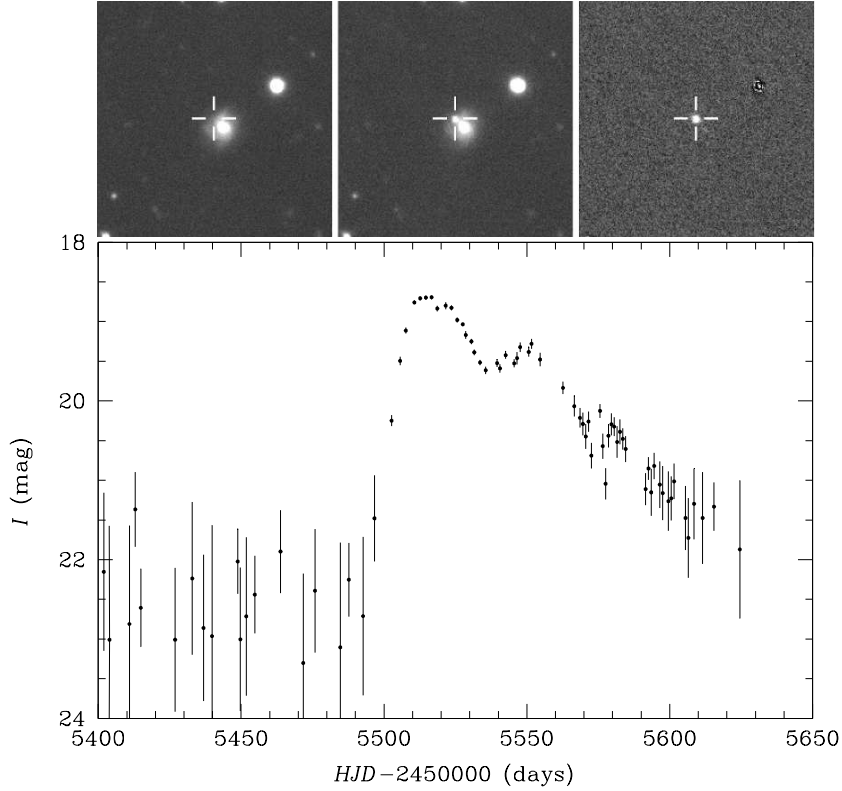
Fig. 4. *Top:* Finding chart for supernova OGLE-2010-SN-060 (MBR104.04.221). The *left image* shows the galaxy before the SN explosion, the *middle image* shows the SN at its peak (marked with cross hairs), and the *right image* shows the difference image. The SN is located $3\overset{''}{.}0$ away from a spiral galaxy. The image covers $60'' \times 60''$. *Bottom:* OGLE-IV light curve for OGLE-2010-SN-060. It peaked at $I = 18.69$ mag on 2010, November 14. The shape of the light curve resembles that of SN Type Ia.

In this study we were interested in finding "all plausible" SNe and transients that would allow us to calibrate our future automatic or semi-automatic pipelines. We found 116 transients (three in overlapping fields) in the standard database and 20 in the new database, of which three were present in the standard database at slightly shifted positions. Often an extended galaxy is split into many "point" sources and the new detection is too far ($> 0\overset{''}{.}5$) from any of the "point" sources to be recognized as an object from the standard database. Such an exploding SN

then affects several nearby sources from the standard database leading to "ghost" variables adjacent to the real variable source. There were 249 such ghost variables. The real variables were recognized by their location on the difference images. After inspecting the light curves we were left with 128 plausible SNe and two foreground dwarf novae (Table 1) based on the light curve shapes. Two spectacular SNe are presented in Figs. 3 and 4, while light curves for basic SN types and two dwarf novae are shown in Fig. 5. Out of 128 galaxies hosting plausible SNe, four have mid-infrared colors consistent with an AGN (see Section 4 for details). These four transients are faint, but two light curves seem to be consistent with SNe and have flat light curves in the present 2012/2013 OGLE-IV season, so we left them on our list of SNe. We removed from that list the two objects that showed further variability in 2012. The remaining light curves were mainly artifacts created by bright stars (moving/rotating spikes), other artifacts associated with variable stars or were caused by photometric problems.
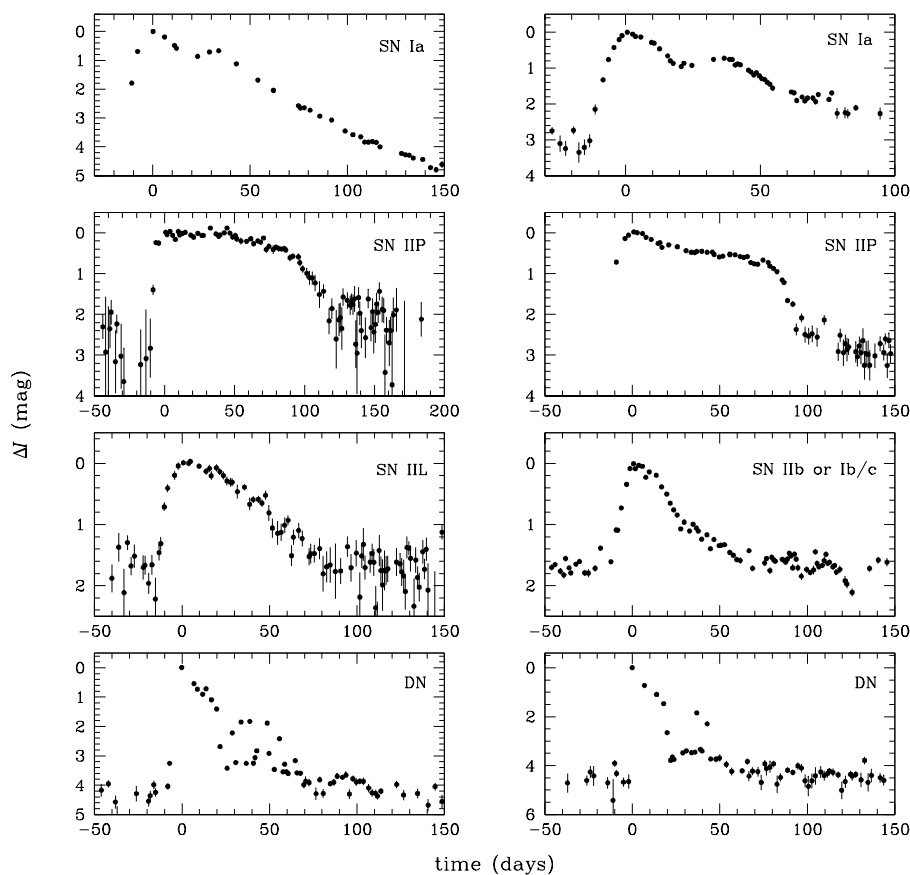

Fig. 5. OGLE-IV light curves for SNe (*three upper rows*) and dwarf novae (*bottom row*). Plausible SN types are based on the light curve shape only and are marked inside panels.

Table 1

OGLE-IV Transients from the OGLE-IV Magellanic Bridge Data

ID	OGLE-IV Object No	RA J2000.0	DEC J2000.0	T_{max} HJD [days]	I^*_{max} [mag]	Rem.
OGLE-2010-SN-002	MBR102.19.2254	$01^{\mathrm{h}}54^{\mathrm{m}}28\!\!\overset{\mathrm{s}}{.}68$	$-72°17'09\!\!\overset{''}{.}5$	245 5378	19.77	G
OGLE-2010-SN-003	MBR110.22.1291	$02^{\mathrm{h}}04^{\mathrm{m}}01\!\!\overset{\mathrm{s}}{.}45$	$-75°21'08\!\!\overset{''}{.}2$	245 5380	20.12	G
OGLE-2010-SN-004	MBR112.03.727	$02^{\mathrm{h}}24^{\mathrm{m}}29\!\!\overset{\mathrm{s}}{.}34$	$-72°57'51\!\!\overset{''}{.}3$	245 5387	20.38	–
OGLE-2010-SN-005	MBR128.28.1045	$03^{\mathrm{h}}11^{\mathrm{m}}25\!\!\overset{\mathrm{s}}{.}82$	$-72°32'31\!\!\overset{''}{.}8$	245 5391	18.68	G
OGLE-2010-SN-006	MBR111.14.313	$02^{\mathrm{h}}16^{\mathrm{m}}14\!\!\overset{\mathrm{s}}{.}06$	$-71°28'23\!\!\overset{''}{.}7$	245 5404	20.34	A
OGLE-2010-SN-007	MBR125.01.1359	$03^{\mathrm{h}}10^{\mathrm{m}}39\!\!\overset{\mathrm{s}}{.}36$	$-76°38'50\!\!\overset{''}{.}9$	245 5404	20.37	–
OGLE-2010-SN-008	MBR144.22.109	$03^{\mathrm{h}}58^{\mathrm{m}}37\!\!\overset{\mathrm{s}}{.}67$	$-74°59'20\!\!\overset{''}{.}6$	245 5404	17.84	G
OGLE-2010-SN-009	MBR118.29.422	$02^{\mathrm{h}}38^{\mathrm{m}}26\!\!\overset{\mathrm{s}}{.}47$	$-72°41'02\!\!\overset{''}{.}4$	245 5405	19.92	G
OGLE-2010-SN-010	MBR122.13.1895	$02^{\mathrm{h}}50^{\mathrm{m}}52\!\!\overset{\mathrm{s}}{.}18$	$-72°35'12\!\!\overset{''}{.}5$	245 5410	20.54	–
OGLE-2010-SN-011	MBR112.20.302	$02^{\mathrm{h}}23^{\mathrm{m}}08\!\!\overset{\mathrm{s}}{.}85$	$-72°27'20\!\!\overset{''}{.}8$	245 5413	19.71	G
OGLE-2010-SN-012	MBR106.04.582	$02^{\mathrm{h}}06^{\mathrm{m}}12\!\!\overset{\mathrm{s}}{.}26$	$-71°09'50\!\!\overset{''}{.}1$	245 5415	19.66	G
OGLE-2010-SN-013	MBR115.29.673	$02^{\mathrm{h}}25^{\mathrm{m}}25\!\!\overset{\mathrm{s}}{.}19$	$-75°49'02\!\!\overset{''}{.}4$	245 5415	20.52	–
OGLE-2010-SN-014	MBR109.31.2418	$02^{\mathrm{h}}00^{\mathrm{m}}52\!\!\overset{\mathrm{s}}{.}95$	$-73°48'13\!\!\overset{''}{.}1$	245 5427	19.60	G
OGLE-2010-SN-015	MBR142.18.476	$03^{\mathrm{h}}57^{\mathrm{m}}18\!\!\overset{\mathrm{s}}{.}30$	$-72°29'51\!\!\overset{''}{.}9$	245 5431	20.53	–
OGLE-2010-SN-016	MBR125.26.1840	$03^{\mathrm{h}}10^{\mathrm{m}}47\!\!\overset{\mathrm{s}}{.}45$	$-75°43'38\!\!\overset{''}{.}6$	245 5435	21.11	–
OGLE-2010-SN-017	MBR110.08.1348	$02^{\mathrm{h}}16^{\mathrm{m}}55\!\!\overset{\mathrm{s}}{.}45$	$-75°37'04\!\!\overset{''}{.}9$	245 5436	21.14	G
OGLE-2010-SN-018	MBR135.03.572	$03^{\mathrm{h}}39^{\mathrm{m}}40\!\!\overset{\mathrm{s}}{.}72$	$-76°43'06\!\!\overset{''}{.}0$	245 5436	20.25	–
OGLE-2010-SN-019	MBR113.05.899	$02^{\mathrm{h}}21^{\mathrm{m}}36\!\!\overset{\mathrm{s}}{.}62$	$-74°11'30\!\!\overset{''}{.}2$	245 5438	20.23	G
OGLE-2010-SN-020	MBR131.08.1684	$03^{\mathrm{h}}27^{\mathrm{m}}34\!\!\overset{\mathrm{s}}{.}72$	$-71°18'44\!\!\overset{''}{.}2$	245 5444	20.11	G
OGLE-2010-SN-021	MBR102.07.858	$01^{\mathrm{h}}44^{\mathrm{m}}43\!\!\overset{\mathrm{s}}{.}87$	$-73°03'36\!\!\overset{''}{.}5$	245 5445	19.52	G
OGLE-2010-SN-022	MBR108.15.690	$01^{\mathrm{h}}59^{\mathrm{m}}57\!\!\overset{\mathrm{s}}{.}91$	$-73°23'34\!\!\overset{''}{.}0$	245 5445	21.11	–
OGLE-2010-SN-023	MBR115.04.680	$02^{\mathrm{h}}24^{\mathrm{m}}59\!\!\overset{\mathrm{s}}{.}23$	$-76°47'15\!\!\overset{''}{.}9$	245 5446	20.29	G
OGLE-2010-SN-024	MBR121.21.889	$02^{\mathrm{h}}50^{\mathrm{m}}29\!\!\overset{\mathrm{s}}{.}28$	$-71°01'31\!\!\overset{''}{.}0$	245 5446	20.00	G
OGLE-2010-SN-025	MBR142.03.946	$03^{\mathrm{h}}53^{\mathrm{m}}50\!\!\overset{\mathrm{s}}{.}18$	$-72°57'50\!\!\overset{''}{.}4$	245 5449	18.36	–
OGLE-2010-SN-026	MBR113.02.1083	$02^{\mathrm{h}}28^{\mathrm{m}}08\!\!\overset{\mathrm{s}}{.}57$	$-74°05'12\!\!\overset{''}{.}1$	245 5450	19.24	G
OGLE-2010-SN-027	MBR121.32.1621	$02^{\mathrm{h}}44^{\mathrm{m}}38\!\!\overset{\mathrm{s}}{.}05$	$-70°42'39\!\!\overset{''}{.}7$	245 5450	20.23	–
OGLE-2010-SN-028	MBR125.30.1229	$03^{\mathrm{h}}00^{\mathrm{m}}36\!\!\overset{\mathrm{s}}{.}10$	$-75°37'36\!\!\overset{''}{.}5$	245 5450	20.23	G
OGLE-2010-SN-029	MBR103.06.2532	$01^{\mathrm{h}}43^{\mathrm{m}}44\!\!\overset{\mathrm{s}}{.}64$	$-74°04'44\!\!\overset{''}{.}7$	245 5452	19.38	G
OGLE-2010-SN-030	MBR117.30.14N	$02^{\mathrm{h}}35^{\mathrm{m}}04\!\!\overset{\mathrm{s}}{.}98$	$-71°28'45\!\!\overset{''}{.}8$	245 5462	19.36	G
OGLE-2010-SN-031	MBR136.27.269	$03^{\mathrm{h}}39^{\mathrm{m}}20\!\!\overset{\mathrm{s}}{.}40$	$-70°15'14\!\!\overset{''}{.}2$	245 5465	19.95	G
OGLE-2010-SN-032	MBR133.26.541	$03^{\mathrm{h}}31^{\mathrm{m}}45\!\!\overset{\mathrm{s}}{.}13$	$-73°19'29\!\!\overset{''}{.}0$	245 5468	20.62	–
OGLE-2010-SN-033	MBR118.27.32N	$02^{\mathrm{h}}42^{\mathrm{m}}30\!\!\overset{\mathrm{s}}{.}47$	$-72°31'23\!\!\overset{''}{.}4$	245 5469	19.17	G
OGLE-2010-SN-034	MBR109.25.2848	$01^{\mathrm{h}}56^{\mathrm{m}}44\!\!\overset{\mathrm{s}}{.}15$	$-74°07'16\!\!\overset{''}{.}4$	245 5470	20.10	G
OGLE-2010-SN-035	MBR111.07.1246	$02^{\mathrm{h}}14^{\mathrm{m}}38\!\!\overset{\mathrm{s}}{.}79$	$-71°41'11\!\!\overset{''}{.}8$	245 5471	20.57	–
OGLE-2010-SN-036	MBR117.21.816	$02^{\mathrm{h}}35^{\mathrm{m}}27\!\!\overset{\mathrm{s}}{.}64$	$-71°43'29\!\!\overset{''}{.}1$	245 5476	20.36	G
OGLE-2010-SN-037	MBR108.29.613	$02^{\mathrm{h}}06^{\mathrm{m}}41\!\!\overset{\mathrm{s}}{.}18$	$-72°46'22\!\!\overset{''}{.}4$	245 5481	18.41	G
OGLE-2010-SN-038	MBR115.06.597	$02^{\mathrm{h}}19^{\mathrm{m}}15\!\!\overset{\mathrm{s}}{.}00$	$-76°46'56\!\!\overset{''}{.}5$	245 5481	19.60	G
OGLE-2010-SN-039	MBR122.08.1171	$03^{\mathrm{h}}00^{\mathrm{m}}49\!\!\overset{\mathrm{s}}{.}14$	$-72°34'35\!\!\overset{''}{.}9$	245 5481	19.39	–
OGLE-2010-SN-040	MBR145.22.290	$04^{\mathrm{h}}03^{\mathrm{m}}44\!\!\overset{\mathrm{s}}{.}04$	$-71°54'42\!\!\overset{''}{.}7$	245 5484	19.62	G
OGLE-2010-SN-041	MBR138.26.198	$03^{\mathrm{h}}44^{\mathrm{m}}25\!\!\overset{\mathrm{s}}{.}87$	$-72°40'30\!\!\overset{''}{.}3$	245 5485	20.23	G
OGLE-2010-SN-042	MBR142.15.1583	$03^{\mathrm{h}}45^{\mathrm{m}}16\!\!\overset{\mathrm{s}}{.}38$	$-72°38'50\!\!\overset{''}{.}0$	245 5485	19.35	G
OGLE-2010-SN-043	MBR144.27.1885	$04^{\mathrm{h}}06^{\mathrm{m}}36\!\!\overset{\mathrm{s}}{.}14$	$-74°25'20\!\!\overset{''}{.}6$	245 5485	20.43	–
OGLE-2010-SN-044	MBR123.27.710	$02^{\mathrm{h}}59^{\mathrm{m}}44\!\!\overset{\mathrm{s}}{.}89$	$-73°14'50\!\!\overset{''}{.}2$	245 5491	17.29	G
OGLE-2010-SN-045	MBR130.18.1249	$03^{\mathrm{h}}25^{\mathrm{m}}41\!\!\overset{\mathrm{s}}{.}43$	$-75°21'51\!\!\overset{''}{.}1$	245 5492	20.63	G
OGLE-2010-SN-046	MBR102.21.2068	$01^{\mathrm{h}}49^{\mathrm{m}}26\!\!\overset{\mathrm{s}}{.}92$	$-72°17'38\!\!\overset{''}{.}9$	245 5493	19.97	G
OGLE-2010-SN-047	MBR136.26.177	$03^{\mathrm{h}}40^{\mathrm{m}}55\!\!\overset{\mathrm{s}}{.}79$	$-70°18'18\!\!\overset{''}{.}1$	245 5494	19.76	G

Table 1

Continued

ID	OGLE-IV Object No	RA J2000.0	DEC J2000.0	T_{max} HJD [days]	I^*_{max} [mag]	Rem.
OGLE-2010-SN-048	MBR100.04.859	$01^h52^m17\!\!\stackrel{s}{.}85$	$-70°36'57\!\!\stackrel{''}{.}1$	245 5497	20.18	G
OGLE-2010-SN-049	MBR142.28.339	$03^h53^m13\!\!\stackrel{s}{.}28$	$-72°11'36\!\!\stackrel{''}{.}3$	245 5498	19.95	G
OGLE-2010-SN-050	MBR141.25.790	$03^h43^m24\!\!\stackrel{s}{.}65$	$-71°05'11\!\!\stackrel{''}{.}9$	245 5500	20.51	G
OGLE-2010-SN-051	MBR135.30.1493	$03^h36^m33\!\!\stackrel{s}{.}32$	$-75°39'37\!\!\stackrel{''}{.}0$	245 5503	20.54	–
OGLE-2010-SN-052	MBR143.14.123	$03^h50^m45\!\!\stackrel{s}{.}59$	$-74°02'14\!\!\stackrel{''}{.}2$	245 5504	19.61	G
OGLE-2010-SN-053	MBR123.11.143	$02^h58^m00\!\!\stackrel{s}{.}77$	$-74°01'59\!\!\stackrel{''}{.}6$	245 5507	18.73	–
OGLE-2010-SN-054	MBR117.28.373	$02^h38^m28\!\!\stackrel{s}{.}17$	$-71°29'21\!\!\stackrel{''}{.}6$	245 5508	21.32	G
OGLE-2010-SN-055	MBR136.03.1063	$03^h37^m55\!\!\stackrel{s}{.}82$	$-71°03'29\!\!\stackrel{''}{.}3$	245 5508	19.61	G
OGLE-2010-SN-056	MBR119.27.1327	$02^h44^m27\!\!\stackrel{s}{.}13$	$-73°46'13\!\!\stackrel{''}{.}8$	245 5509	19.81	G
OGLE-2010-SN-057	MBR104.30.352	$01^h46^m19\!\!\stackrel{s}{.}21$	$-74°33'21\!\!\stackrel{''}{.}5$	245 5510	19.57	–
OGLE-2010-SN-058	MBR131.02.538	$03^h25^m13\!\!\stackrel{s}{.}62$	$-71°50'33\!\!\stackrel{''}{.}1$	245 5515	20.59	–
OGLE-2010-SN-059	MBR127.11.262	$03^h07^m59\!\!\stackrel{s}{.}86$	$-72°05'31\!\!\stackrel{''}{.}2$	245 5516	18.44	G
OGLE-2010-SN-060	MBR104.04.221	$01^h48^m24\!\!\stackrel{s}{.}30$	$-75°32'47\!\!\stackrel{''}{.}3$	245 5517	18.69	G
OGLE-2010-SN-061	MBR106.31.909	$02^h01^m52\!\!\stackrel{s}{.}33$	$-70°04'44\!\!\stackrel{''}{.}3$	245 5526	19.71	G
OGLE-2010-SN-062	MBR108.27.33N	$02^h10^m18\!\!\stackrel{s}{.}20$	$-72°43'26\!\!\stackrel{''}{.}9$	245 5531	17.61	–
OGLE-2010-SN-063	MBR119.02.638	$02^h44^m52\!\!\stackrel{s}{.}44$	$-74°51'32\!\!\stackrel{''}{.}9$	245 5533	19.98	G
OGLE-2010-SN-064	MBR106.06.328	$02^h01^m17\!\!\stackrel{s}{.}18$	$-71°16'44\!\!\stackrel{''}{.}6$	245 5534	20.42	G
OGLE-2010-SN-065	MBR144.26.1005	$04^h08^m12\!\!\stackrel{s}{.}30$	$-74°28'12\!\!\stackrel{''}{.}0$	245 5545	19.42	G
OGLE-2010-SN-066	MBR131.05.1464	$03^h18^m01\!\!\stackrel{s}{.}95$	$-71°43'20\!\!\stackrel{''}{.}1$	245 5547	19.78	–
OGLE-2010-SN-067	MBR100.03.953	$01^h52^m47\!\!\stackrel{s}{.}44$	$-70°33'34\!\!\stackrel{''}{.}4$	245 5548	20.49	G
OGLE-2010-SN-068	MBR116.13.532	$02^h34^m10\!\!\stackrel{s}{.}79$	$-70°52'16\!\!\stackrel{''}{.}2$	245 5550	18.54	G
OGLE-2010-SN-069	MBR119.30.63N	$02^h39^m27\!\!\stackrel{s}{.}11$	$-73°49'23\!\!\stackrel{''}{.}0$	245 5552	19.57	G
OGLE-2010-SN-070	MBR137.27.698	$03^h40^m05\!\!\stackrel{s}{.}51$	$-71°26'13\!\!\stackrel{''}{.}6$	245 5554	19.61	G
OGLE-2010-SN-071	MBR127.23.18N	$03^h02^m23\!\!\stackrel{s}{.}69$	$-71°44'14\!\!\stackrel{''}{.}4$	245 5557	18.80	G
OGLE-2010-SN-072	MBR131.28.564	$03^h22^m49\!\!\stackrel{s}{.}56$	$-70°50'29\!\!\stackrel{''}{.}5$	245 5557	20.07	–
OGLE-2011-SN-007	MBR101.23.216	$01^h47^m38\!\!\stackrel{s}{.}12$	$-71°14'57\!\!\stackrel{''}{.}1$	245 5563	19.42	G
OGLE-2011-SN-008	MBR135.32.2073N	$03^h31^m31\!\!\stackrel{s}{.}90$	$-75°47'42\!\!\stackrel{''}{.}9$	245 5579	19.13	G
OGLE-2011-SN-009	MBR123.32.2468N	$02^h49^m26\!\!\stackrel{s}{.}55$	$-73°22'07\!\!\stackrel{''}{.}6$	245 5582	17.80	G
OGLE-2011-SN-010	MBR129.25.1197N	$03^h02^m59\!\!\stackrel{s}{.}96$	$-74°20'31\!\!\stackrel{''}{.}9$	245 5592	18.49	G
OGLE-2011-SN-011	MBR109.02.53N	$02^h11^m44\!\!\stackrel{s}{.}30$	$-74°47'20\!\!\stackrel{''}{.}3$	245 5593	17.67	G
OGLE-2011-SN-012	MBR138.04.49N	$03^h38^m24\!\!\stackrel{s}{.}06$	$-73°35'19\!\!\stackrel{''}{.}1$	245 5596	18.77	G
OGLE-2011-SN-013	MBR115.24.75N	$02^h18^m53\!\!\stackrel{s}{.}73$	$-76°03'06\!\!\stackrel{''}{.}0$	245 5608	18.39	G
OGLE-2011-SN-014	MBR100.30.381	$01^h49^m58\!\!\stackrel{s}{.}97$	$-69°40'13\!\!\stackrel{''}{.}0$	245 5760	20.08	G
OGLE-2011-SN-015	MBR112.29.656	$02^h22^m46\!\!\stackrel{s}{.}39$	$-71°59'15\!\!\stackrel{''}{.}4$	245 5760	19.88	G
OGLE-2011-SN-016	MBR121.06.52N	$02^h47^m17\!\!\stackrel{s}{.}33$	$-71°49'09\!\!\stackrel{''}{.}8$	245 5761	18.58	–
OGLE-2011-SN-017	MBR127.17.641	$03^h13^m27\!\!\stackrel{s}{.}68$	$-71°48'48\!\!\stackrel{''}{.}5$	245 5785	19.13	G
OGLE-2011-SN-018	MBR123.22.567N	$02^h53^m17\!\!\stackrel{s}{.}38$	$-73°42'54\!\!\stackrel{''}{.}5$	245 5788	18.50	G
OGLE-2011-SN-019	MBR121.07.686	$02^h45^m34\!\!\stackrel{s}{.}06$	$-71°48'25\!\!\stackrel{''}{.}7$	245 5799	19.97	G
OGLE-2011-SN-020	MBR133.24.403	$03^h19^m09\!\!\stackrel{s}{.}15$	$-73°43'36\!\!\stackrel{''}{.}8$	245 5804	21.28	G
OGLE-2011-SN-021	MBR141.24.965	$03^h44^m06\!\!\stackrel{s}{.}00$	$-71°07'56\!\!\stackrel{''}{.}4$	245 5806	19.88	G
OGLE-2011-SN-022	MBR114.20.214	$02^h27^m38\!\!\stackrel{s}{.}11$	$-74°56'55\!\!\stackrel{''}{.}0$	245 5808	20.30	G A
OGLE-2011-SN-023	MBR116.17.1214	$02^h42^m59\!\!\stackrel{s}{.}19$	$-70°27'39\!\!\stackrel{''}{.}0$	245 5811	20.30	–
OGLE-2011-SN-024	MBR110.05.116	$02^h04^m10\!\!\stackrel{s}{.}92$	$-76°10'22\!\!\stackrel{''}{.}3$	245 5812	20.37	G
OGLE-2011-SN-025	MBR117.22.662	$02^h33^m32\!\!\stackrel{s}{.}70$	$-71°46'13\!\!\stackrel{''}{.}1$	245 5812	20.36	G
OGLE-2011-SN-026	MBR126.30.875	$03^h03^m25\!\!\stackrel{s}{.}99$	$-70°05'25\!\!\stackrel{''}{.}0$	245 5812	19.81	G
OGLE-2011-SN-027	MBR130.05.1170	$03^h15^m11\!\!\stackrel{s}{.}01$	$-76°02'45\!\!\stackrel{''}{.}0$	245 5812	19.99	G

Table 1

Concluded

ID	OGLE-IV Object No	RA J2000.0	DEC J2000.0	T_{max} HJD [days]	I^*_{max} [mag]	Rem.
OGLE-2011-SN-028	MBR130.01.1341	$03^{\mathrm{h}}25^{\mathrm{m}}49\!\!^{\mathrm{s}}\!60$	$-76°01'41\!\!''\!1$	245 5813	20.26	G
OGLE-2011-SN-029	MBR145.32.271	$03^{\mathrm{h}}59^{\mathrm{m}}48\!\!^{\mathrm{s}}\!72$	$-71°33'27\!\!''\!4$	245 5817	20.73	G
OGLE-2011-SN-030	MBR102.16.792	$01^{\mathrm{h}}40^{\mathrm{m}}52\!\!^{\mathrm{s}}\!31$	$-72°43'18\!\!''\!7$	245 5830	20.00	G
OGLE-2011-SN-031	MBR144.32.438	$03^{\mathrm{h}}54^{\mathrm{m}}49\!\!^{\mathrm{s}}\!04$	$-74°32'55\!\!''\!6$	245 5833	20.34	G
OGLE-2011-SN-032	MBR102.08.2592	$01^{\mathrm{h}}58^{\mathrm{m}}11\!\!^{\mathrm{s}}\!17$	$-72°32'04\!\!''\!0$	245 5839	20.41	G
OGLE-2011-SN-033	MBR131.30.1305	$03^{\mathrm{h}}18^{\mathrm{m}}26\!\!^{\mathrm{s}}\!34$	$-70°44'07\!\!''\!1$	245 5841	20.51	G
OGLE-2011-SN-034	MBR121.29.882	$02^{\mathrm{h}}50^{\mathrm{m}}18\!\!^{\mathrm{s}}\!34$	$-70°52'25\!\!''\!8$	245 5842	20.12	G
OGLE-2011-SN-035	MBR126.20.189	$03^{\mathrm{h}}08^{\mathrm{m}}05\!\!^{\mathrm{s}}\!00$	$-70°38'26\!\!''\!9$	245 5842	19.94	G
OGLE-2011-SN-036	MBR122.20.1109	$02^{\mathrm{h}}53^{\mathrm{m}}23\!\!^{\mathrm{s}}\!21$	$-72°19'55\!\!''\!7$	245 5845	19.64	G
OGLE-2011-SN-037	MBR123.02.1141	$02^{\mathrm{h}}59^{\mathrm{m}}13\!\!^{\mathrm{s}}\!85$	$-74°11'35\!\!''\!7$	245 5856	20.15	G
OGLE-2011-SN-038	MBR132.04.1169	$03^{\mathrm{h}}21^{\mathrm{m}}24\!\!^{\mathrm{s}}\!93$	$-72°56'09\!\!''\!5$	245 5863	20.30	–
OGLE-2011-SN-039	MBR137.13.246N	$03^{\mathrm{h}}34^{\mathrm{m}}02\!\!^{\mathrm{s}}\!19$	$-72°09'25\!\!''\!1$	245 5865	19.11	G
OGLE-2011-SN-040	MBR118.10.1378	$02^{\mathrm{h}}41^{\mathrm{m}}49\!\!^{\mathrm{s}}\!51$	$-73°09'12\!\!''\!2$	245 5866	20.31	G
OGLE-2011-SN-041	MBR107.04.1444	$02^{\mathrm{h}}05^{\mathrm{m}}13\!\!^{\mathrm{s}}\!75$	$-72°16'28\!\!''\!4$	245 5870	20.54	G
OGLE-2011-SN-042	MBR102.23.1484	$01^{\mathrm{h}}45^{\mathrm{m}}17\!\!^{\mathrm{s}}\!90$	$-72°15'32\!\!''\!6$	245 5871	20.09	G
OGLE-2011-SN-043	MBR119.03.957	$02^{\mathrm{h}}43^{\mathrm{m}}47\!\!^{\mathrm{s}}\!68$	$-74°43'18\!\!''\!6$	245 5871	18.03	G
OGLE-2011-SN-044	MBR106.29.211	$02^{\mathrm{h}}06^{\mathrm{m}}31\!\!^{\mathrm{s}}\!94$	$-70°17'30\!\!''\!8$	245 5874	20.12	G
OGLE-2011-SN-045	MBR126.30.805	$03^{\mathrm{h}}03^{\mathrm{m}}06\!\!^{\mathrm{s}}\!86$	$-70°10'26\!\!''\!3$	245 5874	19.63	G
OGLE-2011-SN-046	MBR138.23.558	$03^{\mathrm{h}}33^{\mathrm{m}}19\!\!^{\mathrm{s}}\!54$	$-72°55'18\!\!''\!8$	245 5874	19.83	G
OGLE-2011-SN-047	MBR102.02.911	$01^{\mathrm{h}}53^{\mathrm{m}}29\!\!^{\mathrm{s}}\!05$	$-73°06'55\!\!''\!1$	245 5879	19.87	G
OGLE-2011-SN-048	MBR128.30.1799	$03^{\mathrm{h}}05^{\mathrm{m}}44\!\!^{\mathrm{s}}\!73$	$-72°38'51\!\!''\!9$	245 5886	20.58	G
OGLE-2011-SN-049	MBR122.26.1156	$02^{\mathrm{h}}59^{\mathrm{m}}04\!\!^{\mathrm{s}}\!44$	$-72°00'29\!\!''\!0$	245 5890	19.09	G
OGLE-2011-SN-050	MBR134.04.906	$03^{\mathrm{h}}31^{\mathrm{m}}27\!\!^{\mathrm{s}}\!83$	$-75°24'23\!\!''\!1$	245 5906	18.80	G
OGLE-2011-SN-051	MBR115.13.276N	$02^{\mathrm{h}}23^{\mathrm{m}}25\!\!^{\mathrm{s}}\!06$	$-76°27'53\!\!''\!3$	245 5910	17.91	G
OGLE-2011-SN-052	MBR121.31.984	$02^{\mathrm{h}}46^{\mathrm{m}}42\!\!^{\mathrm{s}}\!15$	$-70°40'18\!\!''\!7$	245 5910	20.39	G
OGLE-2011-SN-053	MBR139.27.895	$03^{\mathrm{h}}48^{\mathrm{m}}47\!\!^{\mathrm{s}}\!87$	$-73°48'08\!\!''\!8$	245 5925	19.31	–
OGLE-2012-SN-053	MBR102.15.317	$01^{\mathrm{h}}44^{\mathrm{m}}38\!\!^{\mathrm{s}}\!46$	$-72°42'46\!\!''\!6$	245 5929	20.75	G
OGLE-2012-SN-054	MBR120.19.1297	$02^{\mathrm{h}}49^{\mathrm{m}}20\!\!^{\mathrm{s}}\!06$	$-75°24'09\!\!''\!3$	245 5938	19.94	G
OGLE-2012-SN-055	MBR127.02.1343	$03^{\mathrm{h}}09^{\mathrm{m}}49\!\!^{\mathrm{s}}\!04$	$-72°15'18\!\!''\!9$	245 5938	20.00	G
OGLE-2012-SN-056	MBR129.02.121	$03^{\mathrm{h}}17^{\mathrm{m}}20\!\!^{\mathrm{s}}\!34$	$-74°52'10\!\!''\!1$	245 5942	19.25	G
OGLE-2012-SN-057	MBR140.30.903	$03^{\mathrm{h}}47^{\mathrm{m}}15\!\!^{\mathrm{s}}\!56$	$-75°00'05\!\!''\!4$	245 5948	20.07	G
OGLE-2012-SN-058	MBR123.09.1095	$03^{\mathrm{h}}03^{\mathrm{m}}01\!\!^{\mathrm{s}}\!93$	$-73°51'11\!\!''\!4$	245 5964	19.87	–
OGLE-2012-SN-059	MBR102.06.2066	$01^{\mathrm{h}}46^{\mathrm{m}}08\!\!^{\mathrm{s}}\!74$	$-72°55'43\!\!''\!5$	245 5982	20.12	G
OGLE-2012-SN-060	MBR145.30.487	$04^{\mathrm{h}}03^{\mathrm{m}}51\!\!^{\mathrm{s}}\!59$	$-71°30'42\!\!''\!2$	245 5983	20.04	–
Dwarf Nova	MBR124.21.11N	$02^{\mathrm{h}}59^{\mathrm{m}}28\!\!^{\mathrm{s}}\!56$	$-74°48'25\!\!''\!1$	245 5414	16.15	–
Dwarf Nova	MBR120.21.138N	$02^{\mathrm{h}}44^{\mathrm{m}}25\!\!^{\mathrm{s}}\!24$	$-75°33'29\!\!''\!9$	245 5802	15.89	–
AGN	MBR134.31.146	$03^{\mathrm{h}}26^{\mathrm{m}}47\!\!^{\mathrm{s}}\!14$	$-74°37'51\!\!''\!8$	245 5459	19.08	G A
AGN	MBR140.05.1125	$03^{\mathrm{h}}48^{\mathrm{m}}38\!\!^{\mathrm{s}}\!86$	$-76°03'36\!\!''\!1$	245 5445	20.05	A

Notes. *The peak SNe magnitudes were corrected to show only SNe fluxes (the median baseline fluxes were removed). In the first column (ID) the supposedly missing SN numbers at the beginning of each year were already reported in other OGLE papers. In the second column (OGLE-IV Object No) objects ending with an "N" are discovered in the database of new objects. The remaining objects were found in the standard database. In the last column (Remarks) "G" means that the SN host galaxy is present on the template image ($I < 21$ mag) and "A" means that the WISE $W1 - W2$ color of the host galaxy is consistent with an AGN (see Section 4).

3.   SN Numbers

In this section, we estimate the number of expected SNe as a function of magnitude (based on available SNe rates) and hence the OGLE-IV SN detection efficiency. A source of absolute magnitude M_I is observed at magnitude

$$m_I = M_I + 5\log d(z,\Omega_X) + 25 + A_{\mathrm{Galaxy}} + A_{\mathrm{Host}}(z) + K(z, A_{\mathrm{Host}}(z)) \qquad (2)$$

where $d(z,\Omega_X)$ is the luminosity distance in Mpc, a function of redshift z and cosmological model Ω_X, A_{Galaxy} and $A_{\mathrm{Host}}(z)$ are the extinctions in our own Galaxy and in the SN host galaxy, respectively, and $K(z, A_{\mathrm{Host}}(z))$ is the single filter K-correction (see Kim, Goobar and Perlmutter 1996 and Nugent, Kim and Perlmutter 2002). We used a standard ΛCDM cosmological model with $(\Omega_\Lambda, \Omega_M, \Omega_k) = (0.7, 0.3, 0.0)$ and $h = H_0/(100\,\mathrm{km\,s^{-1}\,Mpc^{-1}}) = 0.73$ to calculate distances. The Galactic extinction was set to $A_{\mathrm{Galaxy}} = 0.11$ mag (Schlegel, Finkbeiner and Davis 1998) and, for simplicity, the median SNe Type Ia and ccSNe host extinctions were assumed to be $A_{\mathrm{Host\ SNIa}} = 0.08$ mag and $A_{\mathrm{Host\ ccSNe}} = 0.22$ mag at $z = 0$ (*e.g.*, Holwerda 2008 and Schmidt *et al.* 1994, respectively). The host extinctions at different redshifts in filter *I* were calculated using a standard extinction law with $R_V = 3.1$. To calculate *K*-corrections (Fig. 6), we used the SN spectral templates for the peak brightness from Peter Nugent's spectral templates website[†] and the formula for the single filter *K*-correction from Kim, Goobar and Perlmutter (1996; their Eq. 1). Because OGLE SNe light curves often contain both flux from SNe and their host galaxies, the peak magnitudes were corrected to show only SNe fluxes (median baseline fluxes were removed).

3.1.   *The Expected SN Numbers*

There are two ways to obtain the SNe detection efficiency for a survey. The first one is to simulate SN light curves of various types with the OGLE-IV cadence and photometric properties, and check if they pass our "bump" test (Section 2). Such a simulation is difficult to perform due to many input unknowns and the interpretation may be ambiguous. While we are interested in SNe light curves only, they often include flux coming from host galaxies. It is unknown what fraction of light coming from a galaxy should be added to the SN light, since some SNe explode in the outskirts of galaxies some near centers, SNe span a wide range of brightness, and one has to include extinctions. This would require simulating images of galaxies with exploding SNe and then running through standard OGLE-IV photometric pipelines. The second problem is that it is necessary to assume some fractions of different types of SNe to a limiting magnitude (explained in details in the second simulation) to calculate a proper SNe detection efficiency of a survey. Therefore, we decided to perform a different simulation, where we compare our number of SNe (their peak magnitudes) with simulated number of SNe to a given limiting peak magnitude.

[†]*http://supernova.lbl.gov/∼nugent/nugent_templates.html*
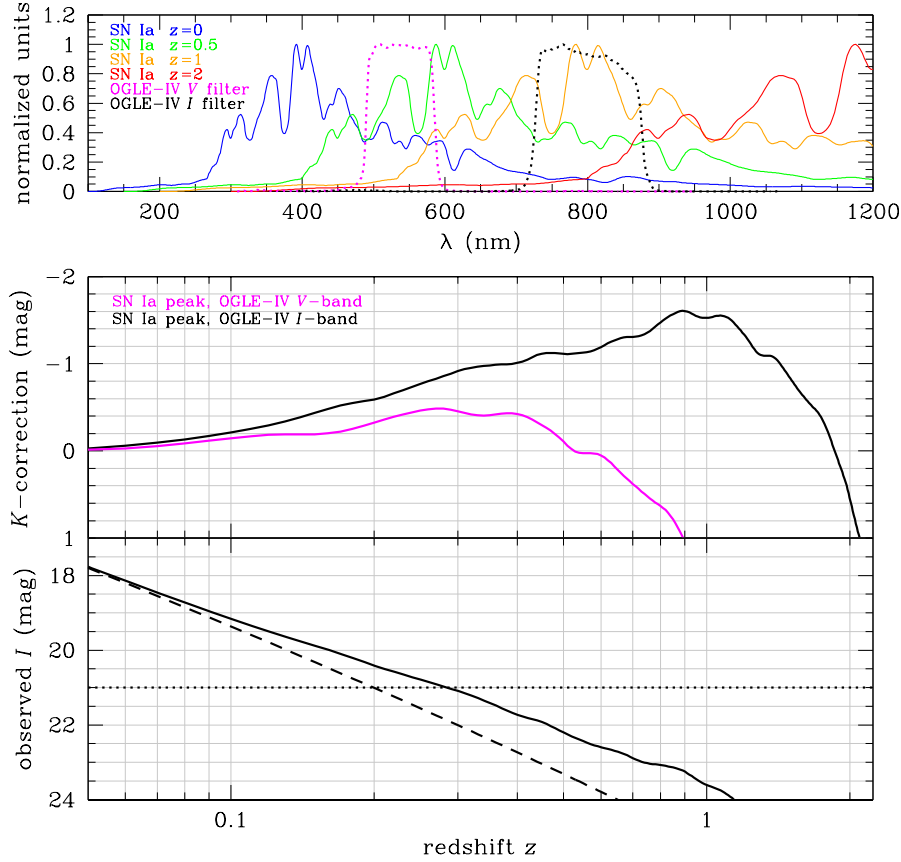
Fig. 6. Impact of redshift on the observed properties of SN Type Ia. *Top:* SN Type Ia peak spectrum ($t = 0$ days) shown at four redshifts $z = 0$, 0.5, 1, and 2 (blue, green, yellow, and red lines, respectively). We also show the OGLE-IV *V*- and *I*-band filter transmission fractions convolved with the quantum efficiency of the OGLE-IV CCDs (dotted magenta and black, respectively). Both the SN spectra and filter transmissions are normalized to 1. *Middle: K*-corrections for the SN Type Ia peak spectrum ($t = 0$ days) as a function of redshift for the *V*- and *I*-band filters (solid magenta and black, respectively). The *I*-band absolute brightness of SN Type Ia increases with increasing redshift, with *K*-corrections peaking at $K \approx -1.6$ mag for $z \approx 0.9$, and then decreases when the spectrum peak leaves the *I*-band filter ($z > 1$). *Bottom:* The observed *I*-band peak magnitudes as a function of redshift (solid line). The dashed line is for the observed *I*-band peak magnitudes with no *K*-corrections. The negative *K*-correction increases the limiting redshift from 0.20 to 0.28 given the OGLE-IV magnitude limit of $I \approx 21$ mag (horizontal dotted line), tripling the effective survey volume.

To calculate the expected number of SNe as a function of *I*-band limiting peak magnitude (Fig. 7), we used the volumetric SN rates from Li *et al.* (2011a). For the SN Type Ia, Ibc, and II, we used SN rates of 0.301×10^{-4} SN yr^{-1} Mpc^{-3}, 0.258×10^{-4} SN yr^{-1} Mpc^{-3}, and 0.447×10^{-4} SN yr^{-1} Mpc^{-3}, respectively, that evolve with redshift as $\propto (1 + z)^{3.6}$. We also used the fractions of various SNe within core-collapse group from Li *et al.* (2011b), namely IIP (70%), IIL (10%), IIb (12%), and IIn (9%).
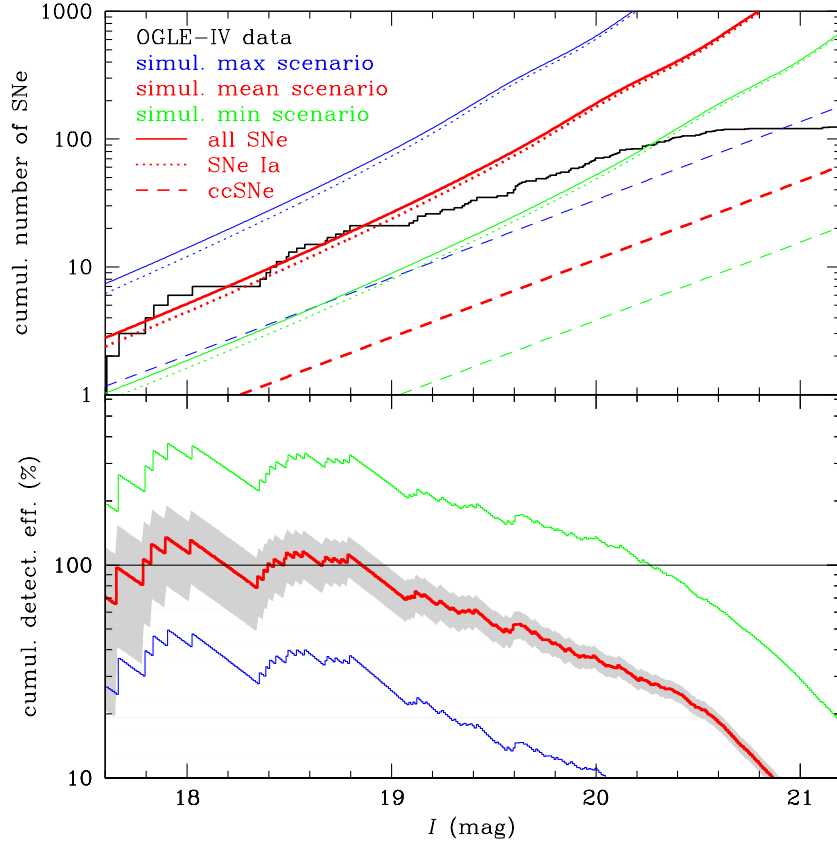
Fig. 7. *Top.* Cumulative number of SNe discovered by OGLE-IV as a function of the limiting peak *I*-band magnitude (black solid line). Solid color lines show the total number of predicted SNe, while the dotted line is for SNe Type Ia only and dashed line is for core-collapse SNe. Red color marks the prediction for typical absolute peak magnitudes and typical volumetric rates. Blue and green colors mark the optimistic (absolute magnitudes brighter and volumetric SNe rates higher than in a typical scenario) and pessimistic scenarios, respectively (see text for details). *Bottom.* Cumulative detection efficiency of SNe as a function of a limiting peak *I*-band magnitude. Line styles and color coding is identical as in the *top panel*. The gray area reflects the 1σ Poisson uncertainties for the typical scenario (red).

The peak *I*-band magnitude for SN Type Ia was taken from Riess, Press and Kirshner (1996) and was set to $M_I = -19.05$ mag. We simplified our calculations by combining SNe Type Ib, Ic, and Ibc into one group for which we set the peak magnitude to $M_I = -16.7$ mag, converting M_R from Li *et al.* (2011b). For SN Type II, we adopt $M_I = -17.6$ mag, -18.05 mag, and -17.4 mag for SN Type IIP, IIL, and IIb/IIn, respectively. The value for SN Type IIP is consistent with Otsuka *et al.* (2012) and the value for SN Type IIb consistent with Tsvetkov *et al.* (2012), SN Type IIn span a huge range of absolute magnitudes (-15 to -23) and our choice differs from the average of $M_I = -18.9$ mag adopted in Kiewe *et al.* (2012).

With the exception of SN Type Ia, the distribution of absolute magnitudes for each SN type is not precisely known. There is no evidence that they are Gaussian, so we estimated the maximum and minimum number of expected SNe (hereafter referred to as the optimistic and pessimistic scenarios), by taking into account the uncertainties in rates and peak magnitudes. For SN Type Ia, we adopted the range of I-band magnitudes of ± 0.5 mag, for Type Ibc ± 0.4 mag, for Types IIP ± 0.6 mag, IIL ± 0.3 mag and IIb/n ± 0.8 mag. For the optimistic (pessimistic) scenario, we simply made all SNe brighter (fainter) by the corresponding magnitude shift while simultaneously increased (decreased) the SN rates by their reported uncertainties.

We analyzed two OGLE-IV MBR seasons. The seasonal gaps account for 35% of time annually, so the "OGLE-IV SNe MBR season length" accounts for 65% of the year. Our simulated SNe numbers are then calculated for 1.3 year.

Table 2

Cumulative estimated number of SNe per 100 deg^2 per year to the limiting peak magnitude I

Peak	Total SN Number			Cumulative Detection	OGLE-IV SN Number*		
I [mag]	All SNe	SNe Ia	ccSNe	Efficiency (%)	All SNe	SNe Ia	ccSNe
17.0	1	1	0	100	1	1	0
17.5	3	2	1	100	2	1	1
18.0	6	5	1	100	4	3	1
18.5	14	12	2	100	9	8	1
19.0	31	28	3	83	17	15	2
19.5	78	71	7	58	30	27	3
20.0	224	211	13	38	56	53	3
20.5	589	562	27	21	83	79	4

Notes. *The reported SNe numbers are corrected for the OGLE-IV SNe "season length" ($\approx 65\%$ of year).

We show the results of our simulations in Fig. 7 and Table 2. Our SNe search is $\approx 100\%$ complete for $I < 18.8$ mag and drops to 50% at $I \approx 19.7$ mag. In Table 2, we show the expected number of SNe per 100 deg^2 per year as a function of the limiting magnitude both for the OGLE-IV survey setup and absolute numbers.

4. Discriminating SNe from AGNs

AGNs are optically variable and increase our false-positive rate, especially since we detect many "transients" near the centers of galaxies. A key point is that bright and/or extended galaxies are usually split into many "point" sources by our pipeline, so that even for bright galaxies there may be no detection of an object at the galaxy's center in the standard database and a transient can appear as new object.

One of the key features of AGNs is their dust emission at mid-infrared (mid-IR) wavelengths. The mid-IR colors of quasars are well established from modern space missions (see Stern *et al.* 2005, Assef *et al.* 2010, Kozłowski *et al.* 2010a, Stern *et al.* 2012) such as Spitzer Space Telescope and Wide-field Infrared Survey Explorer (WISE, Wright *et al.* 2010). WISE observed the whole sky at 3.4 μm, 4.6 μm, 12 μm, and 22 μm, hereafter called $W1$, $W2$, $W3$, and $W4$ bands, respectively, and is an ideal source permitting removal of AGNs from our sample. Stern *et al.* (2012) proposed a simple cut based on $W1$ and $W2$ bands, namely $W1 - W2 \geq 0.8$ mag, that selects 78% AGNs with 95% reliability for $W2 \lesssim 15.0$ mag. The remaining two bands are not nearly as sensitive as the first two, and were not used. Assef *et al.* (2012), based on ≈ 1000 AGNs from the 9 deg^2 NOAO Bootes Field, proposed another relation that goes 2 mag deeper than that of Stern *et al.* (2012), $W1 - W2 > 0.53 \times \exp\left(0.18 \times (W2 - 13.76)\right)$ mag for $W2 < 17.11$ mag that returns AGN with 75% reliability. Their second and more stringent relation (90% reliability) is not used here, since we are not interested in reliably identifying AGNs, but rather in discriminating plausible AGNs.
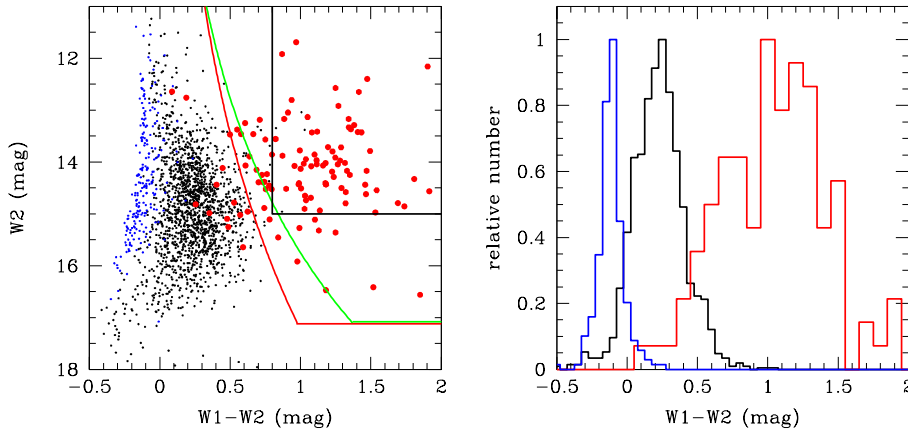
Fig. 8. *Left:* WISE color–magnitude diagram for a subset of the OGLE-IV GSEP stars (blue), galaxies (black), and OGLE-III LMC AGNs (red). The black lines mark the Stern *et al.* (2012) AGN selection region, the red (green) lines mark the Assef *et al.* (2012) AGN selection region for 75% (90%) reliability. Both selection methods identify the majority of the known AGNs. *Right:* Normalized histograms for OGLE-IV GSEP stars (blue), galaxies (black), and OGLE-III LMC AGNs (red). Median WISE $W1 - W2$ colors are -0.12 mag, 0.22 mag, and 1.07 mag, respectively.

We matched the OGLE-III LMC confirmed quasars (Kozłowski *et al.* 2012), galaxies detected in the OGLE-IV GAIA South Ecliptic Pole fields (GSEP, Soszyński *et al.* 2012), and a subset of GSEP stars to the WISE mid-IR database to verify these relations (Fig. 8).

Of the 169 LMC quasars, we matched 111 (66%) to WISE (3″ matching radius), where 98 meet the second criterion ($W2 \lesssim 15.0$ mag) from Stern *et al.* (2012) and all of them are brighter than $W2 = 17.11$ mag (second criterion from Assef *et al.* 2012). Both samples span $0.09 < W1 - W2 < 1.92$ mag, with the medians

$W1 - W2 = 1.07$ mag and $W1 - W2 = 1.04$ mag, respectively. The first criterion of Stern *et al.* (2012) selects 70 AGNs (71% of the sample) and the first criterion of Assef *et al.* (2012) selects 98 (88% of the sample). We therefore adopted the Assef *et al.* (2012) method to eliminate AGNs from our sample.

We used the AGN and Galaxy Ages Survey (AGES) deep data (Kochanek *et al.* 2012) to study the depth of WISE for AGNs in the OGLE-IV Magellanic Bridge data. We selected objects with AGES flags $QSO = 1$ and/or $AGN = 1$, spectrum redshift $z > 0.6$ to avoid galaxies, and Spitzer colors $[3.6] - [4.5] > 0.5$ mag to avoid stars and galaxies, as AGNs. The faintest objects reached $I < 22.5$ mag, *i.e.*, ≈ 2.5 mag deeper than OGLE. The Spitzer $[4.5]$ band is nearly identical to WISE $W2$ channel with only 3% magnitude differences for AGNs up to $z = 4.5$, so we explicitly assumed them here as equal. The Magellanic Bridge is located close to the South Ecliptic Pole, where WISE obtained the highest number of epochs. At the center (further edge) of the Magellanic Bridge, WISE obtained > 30 (> 20) images and the signal-to-noise ratio of 3 is reached at $W1 < 18.7$ mag and $W2 < 17.2$ mag ($W1 < 18.4$ mag and $W2 < 17.0$ mag). The average AGN $I - W2$ color is 4.7 mag, with the 1σ range of $3.8 < I - W2 < 5.5$ mag. Taking into account both OGLE and WISE depths, we should be finding 94% of AGNs, as compared to fixing the AGES *I*-band magnitude to the OGLE limit and leaving the WISE limit unconstrained.

We matched 1924 galaxies from the OGLE-IV LMC GSEP catalog to the WISE catalog using a $5''$ search radius. There were 1658 matches with a median color $W1 - W2 = 0.22$ mag. We also matched 300 stars with $15 < I < 17$ mag from the OGLE-IV LMC GSEP catalog and 228 stars were matched within $3''$ radius. Their median color is $W1 - W2 = -0.12$ mag. In the right panel of Fig. 8, we show $W1 - W2$ histograms for the three types of objects discussed here. It is clear that even with as simple cut as proposed by Stern *et al.* (2012), we can safely remove the majority of AGNs.

5. OGLE Transient Detection System

In October 2012, we implemented the OGLE-IV Transient Detection System (OTDS) running in a near-real-time at the Warsaw telescope in Las Campanas Observatory, Chile. Its full description will be presented in a forthcoming paper, so we only outline the procedure here.

Raw images are reduced on-the fly, but we run the OTDS pipeline to search for transients just after the last reduction of the night is done and the databases are updated. The lag between taking an image and updating the database can then take up to 24 hours. The OTDS works twofold. First, we inspect a list of new objects with at least two detections at the same location occurring in subsequent images daily. Currently, we only investigate *I*-band images as the bulk ($\approx 90\%$) of observations are obtained with this filter. This includes checking the light curves and both template, original and subtracted (difference) images. We produce light curves for all

promising objects to check their behavior prior to the candidate transient. Second, we will search for SNe in the standard database (not implemented yet). Both approaches will return real SNe or Novae but also spurious detections, such as cosmic rays, photometric problems as well as sometimes variable stars, AGNs and asteroids. Cosmic rays (hitting twice at the same spot!) and subtraction artifacts are by far the most common sources of contamination and are removed automatically using a self-organizing map (SOM) technique (*e.g.*, Wyrzykowski and Belokurov 2008). We then concentrate on discriminating SNe from other real sources such as AGNs (Section 4).

During last three months of 2012, we discovered (or co-discovered) 52 SNe using OTDS. Several of them have been spectroscopically observed and subsequently confirmed by PESSTO collaboration. For example, OGLE-2012-SN-032 and OGLE-2012-SN-007 turned out to be of Type Ia (Anderson *et al.* 2012b), OGLE-2012-SN-005 is also SN Type Ia (Anderson *et al.* 2012a), and OGLE-2012-SN-032 is either SN Type Ia or Ic (Marchi *et al.* 2012). OGLE-2012-SN-014 (SN Ia) is also known as SN 2012fu (Maza *et al.* 2012) and OGLE-2012-SN-009 (SN Ia) that peaked at $I \approx 14.9$ mag is known as SN 2012dk (Bock, Parrent, and Howell 2012). OGLE-2012-SN-051 is a Type Ia SN (Taddia *et al.* 2013) so is OGLE-2012-SN-049, while OGLE-2012-SN-048 and OGLE-2012-SN-050 are both SN Type IIn (Sollerman *et al.* 2013).

6. Summary

In this paper, we presented the results of our search for transients in the OGLE-IV fields located between the Magellanic Clouds. We discovered 126 SNe, two dwarf novae, and two AGNs, while inspecting $\approx 70\,000$ pre-selected two-year-long light curves from ≈ 65 deg^2 of the OGLE-IV Magellanic Bridge data. Based on the known SNe rates, SNe absolute magnitudes, galactic and host extinctions, and calculated *K*-corrections, we simulated the expected numbers of SNe in our survey. We then compared our cumulative number of SNe as a function of *I*-band magnitude to the simulated one, finding that our SNe detection efficiency is very high for $I < 18.8$ mag.

Since establishing OTDS in October 2012, we have discovered 52 new SNe. This number will increase quickly, as the number of observed fields increases to a total of ≈ 600 deg^2. All these discoveries are published on-line on the OGLE web page. In the future, for the brightest and spectroscopically confirmed SNe it will be possible to create high-cadence, well-calibrated light curve templates for various SNe types. All data presented in this paper are available to the astronomical community from the OGLE Internet archive accessible from the OGLE WWW Page or directly:

http://ogle.astrouw.edu.pl
ftp://ftp.astrouw.edu.pl/ogle/ogle4/transients/SN/MBR

Please read the README file for the details on the data presented there as well as on all updates.

The OTDS transients are available from the following webpage:

http://ogle.astrouw.edu.pl/ogle4/transients/

REFERENCES

Anderson, J., *et al.* 2012a, *ATel*, 4594.
Anderson, J., *et al.* 2012b, *ATel*, 4602.
Assef, R.J., *et al.* 2010, *ApJ*, **713**, 970.
Assef, R.J., *et al.* 2012, arXiv:1209.6055.
Astier, P., *et al.* 2006, *A&A*, **447**, 31.
Bock, G., Parrent, J.T., and Howell, D.A. 2012, *CBET*, 3168.
Conley, A., *et al.* 2011, *ApJS*, **192**, 1.
Cooke, J., Sullivan, M., Barton, E.J., Bullock, J.S., Carlberg, R.G., Gal-Yam, A., and Tollerud, E. 2009, *Nature*, **460**, 237.
Cooke, J., *et al.* 2012, *Nature*, **491**, 228.
Drake, A., *et al.* 2009, *ApJ*, **696**, 870.
Grogin, N.A., *et al.* 2011, *ApJS*, **197**, 35.
Hamuy, M., and Pinto, P.A. 2002, *ApJ*, **566**, L63.
Holwerda, B.W. 2008, *MNRAS*, **386**, 475.
Jennings, Z.G., Williams, B.F., Murphy, J.W., Dalcanton, J.J., Gilbert, K.M., Dolphin, A.E., Fouesneau, M., and Weisz, D.R. 2012, *ApJ*, **761**, 26.
Kiewe, M., *et al.* 2012, *ApJ*, **744**, 10.
Kim, A., Goobar, A., and Perlmutter, S. 1996, *PASP*, **108**, 190.
Kochanek, C.S., Beacom, J.F., Kistler, M.D., Prieto, J.L., Stanek, K.Z., Thompson, T.A., and Yüksel, H. 2008, *ApJ*, **684**, 1336.
Kochanek, C.S., *et al.* 2012, *ApJS*, **200**, 8.
Kochanek, C.S., Szczygieł, D.M., and Stanek, K.Z. 2012, *ApJ*, **758**, 142.
Koekemoer, A.M., *et al.* 2011, *ApJS*, **197**, 36.
Kozłowski, S., *et al.* 2010a, *ApJ*, **716**, 530.
Kozłowski, S., *et al.* 2010b, *ApJ*, **722**, 1624.

Kozłowski, S., *et al.* 2012, *ApJ*, **746**, 27.

Law, N.M., *et al.* 2009, *PASP*, **121**, 1395.

Li, W., Chornock, R., Leaman, J., Filippenko, A.V., Poznanski, D., Wang, X., Ganeshalingam, and M., Mannucci, F. 2011a, *MNRAS*, **412**, 1473.

Li, W., *et al.* 2011b, *MNRAS*, **412**, 1441.

Marchi, S., *et al.* 2012, *ATel*, 4558.

Maza, J., *et al.* 2012, *CBET*, 3280.

Nugent, P., Kim, A., and Perlmutter, S. 2002, *PASP*, **114**, 803.

Otsuka, M., *et al.* 2012, *ApJ*, **744**, 26.

Pastorello, A., *et al.* 2007, *Nature*, **447**, 829.

Perlmutter, S., *et al.* 1999, *ApJ*, **517**, 565.

Phillips, M.M. 1993, *ApJ*, **413**, L105.

Poznanski, D., Nugent, P.E., and Filippenko, A.V. 2010, *ApJ*, **721**, 956.

Prieto, J.L., Stanek, K.Z., and Beacom, J.F. 2008, *ApJ*, **673**, 999.

Riess, A.G., Press, W.H., and Kirshner, R.P. 1996, *ApJ*, **473**, 88.

Riess, A.G., *et al.* 1998, *AJ*, **116**, 1009.

Riess, A.G., *et al.* 2001, *ApJ*, **560**, 49.

Schmidt, B.P., Kirshner, R.P., Eastman, R.G., Phillips, M.M., Suntzeff, N.B., Hamuy, M., Maza, J., and Aviles, R. 1994, *ApJ*, **432**, 42.

Schlegel, D.J., Finkbeiner, D.P., and Davis, M. 1998, *ApJ*, **500**, 525.

Silk, J. 2005, *MNRAS*, **364**, 1337.

Smartt, S.J. 2009, *Ann. Rev. Astron. Astrophys.*, **47**, 63.

Smartt, S.J., Eldridge, J.J., Crockett, R.M., and Maund, J.R. 2009, *MNRAS*, **395**, 1409.

Smith, N., Li, W., Silverman, J.M., Ganeshalingam, M., and Filippenko, A.V. 2011, *MNRAS*, **415**, 773.

Sollerman, J., *et al.* 2013, *ATel*, 4696.

Soszyński, I., *et al.* 2012, *Acta Astron.*, **62**, 219.

Stern, D., *et al.* 2005, *ApJ*, **631**, 163.

Stern, D., *et al.* 2012, *ApJ*, **753**, 30.

Stoll, R., Prieto, J.L., Stanek, K.Z., Pogge, R.W., Szczygieł, D.M., Pojmański, G., Antognini, J., and Yan, H. 2011, *ApJ*, **730**, 34.

Suzuki, N., *et al.* 2012, *ApJ*, **746**, 85.

Taddia, F., *et al.* 2013, *ATel*, 4698.

Tsvetkov, D.Yu., Volkov, I.M., Sorokina, E.I., Blinnikov, S.I., Pavlyuk, N.N., and Borisov, G.V. 2012, arXiv:1207.2241.

Udalski, A., Szymański, M., Kaluzny, J., Kubiak, M., Krzemiński, W., Mateo, M., Preston, G.W., and Paczyński, B. 1993, *Acta Astron.*, **43**, 289.

Udalski, A. 2003, *Acta Astron.*, **53**, 291.

Udalski, A. 2004a, *IAUC*, 8276.

Udalski, A. 2004b, *IAUC*, 8292.

Udalski, A., *et al.* 2008, *Acta Astron.*, **58**, 69.

Woosley, S.E., and Weaver, T.A. 1986, *Annual Rev. Astron. Astrophys.*, **24**, 205.

Woźniak, P.R. 2000, *Acta Astron.*, **50**, 421.

Wyrzykowski, Ł., and Belokurov, V. 2008, *AIPC*, **1082**, 201.

Wyrzykowski, Ł., *et al.* 2009, *MNRAS*, **397**, 1228.

Wyrzykowski, Ł., Udalski, A., and Kozłowski, S. 2012, *ATel*, 4495.

Wright, E. L., *et al.* 2010, *AJ*, **140**, 1868.